Discovering Associations between Acoustic Emission and Magnetic Resonance Imaging Biomarkers from 10 Osteoarthritic Knees

Lik-Kwan Shark*, *Member, IEEE,* Wei Quan, Michael A. Bowes, John C. Waterton, and John Goodacre

***Abstract*— *Objective*: Acoustic emission (AE) sensed from knee joints during weight-bearing movements greatly increases with joint deterioration, but the relationship between AE patterns and specific anatomical damage, as seen for example in magnetic resonance imaging (MRI), is unknown. This knowledge is essential to validate AE biomarkers for the evaluation of knee joints, and forms the objective of this exploratory work to associate knee AE and MRI. *Methods*: A novel processing framework is proposed to enable direct correlation between static 3D MRI of knees and their dynamic 1D AE during sit-stand-sit movements. It comprises a method to estimate articular cartilage thickness according to joint angle from knee MRI, and a method to derive statistically representative waveform features according to joint angle from movement and load-dependent knee AE. *Results*: In 10 subjects diagnosed with knee osteoarthritis, age 55~79 years and body mass index 25~35 kg/m^2, a strong inverse relationship between knee AE and cartilage thickness in the medial tibiofemoral compartment around the fully standing position was observed. Knees with thinner articular cartilage generated more AE with higher amplitude, greater energy, longer duration, and higher frequencies, in agreement with the assumption of more intense articulation friction under full body weight. *Conclusion*: AE provides promising quantitative biomarkers in knee joint disease. *Significance*: These findings provide impetus for the further development of AE as a low-cost non-invasive biomarker modality to improve the management of knee joint disease.**

***Index Terms*—Acoustic emission, cartilage thickness, knee osteoarthritis, magnetic resonance imaging, medial tibiofemoral joint, sit-stand-sit movement, waveform feature.**

I. Introduction

HEALTHY articular cartilage is a key component in joint mobility. Knee articular cartilage covers the articulating surfaces of the femur, tibia and patella, providing a viscoelastic surface to enable smooth joint movement with minimal friction [1]. During daily activities, the knee is repeatedly exposed to heavy loads and stress, which often reach several times body weight [2]. Degeneration of articular cartilage is a key feature of osteoarthritis (OA) [3]. A common site for the initiation of knee OA is the medial tibiofemoral (MTF) joint [4], often associated with varus malalignment.

Several imaging modalities enable quantitative evaluation of knee OA [5]. Due to wide availability and cost-effectiveness, X-radiography is routine in clinical practice, with diagnosis of knee OA based upon radiographic biomarkers and pain symptoms [6]. X-ray biomarkers are relatively independent of pain symptoms [7], but mainly assess bony tissues with limited prognostic value in early OA. Magnetic resonance imaging (MRI) biomarkers are promising for quantitative evaluation of knee OA [8], [9], as they assess relevant soft tissues in three dimensions. Importantly for longitudinal studies, they do not require ionizing radiation. Some MRI biomarkers, such as bone marrow lesions and synovitis, show moderately good correlation with symptoms [10]-[13].

Nevertheless, there is an inherent limitation in static imaging for quantitative evaluation of knee OA, because it is based on a "snapshot" of the knee in a fixed and (in the case of MRI) unloaded pose. This has led to the development of a complementary non-invasive approach based on sensing of knee joint sounds generated during movements, since an unhealthy knee covered by rough and poorly lubricated cartilage surface should sound noisier than a normal knee [14]. Based on the frequency range, knee joint sounds during movements can be categorized as vibroarthrography which uses accelerometers to capture vibration frequencies below 1 kHz [15]; phonoarthrography which uses microphones to capture audible frequencies in the sonic range (up to 20 kHz) [16]; and acoustic emission (AE) which uses piezoelectric transducers to capture inaudible frequencies in the ultrasonic range (above 20 kHz) [17]. Based on signal processing and analysis from *in vivo* sensing of various knee movements, all three techniques have demonstrated the diagnostic potential for knee joint assessment in terms of differentiating healthy and pathological joints [15], [18], along with the development of novel sensors and wearable systems [19], [20].

Although knee joint sounds can be generated by knee movements performed with or without weight-bearing, loaded movements have been shown to generate more prominent knee

This work was supported by the Medical Research Council in the UK under Grant MR/K025597/1.

*L.-K. Shark is with the Applied Digital and Image Processing Research Centre (ADSIP), School of Engineering, University of Central Lancashire, Preston, UK, (e-mail: LShark@uclan.ac.uk)

W. Quan is with ADSIP, School of Engineering, University of Central Lancashire, Preston, UK.

M. A. Bowes is with Stryker Corp., Manchester, UK.

J. C. Waterton is with Manchester Academic Health Sciences Center, University of Manchester, UK.

J. Goodacre is with Faculty of Health and Medicine, Lancaster University, Lancaster, UK.

joint sounds than unloaded movements [21]-[23], with a potential to offer higher sensitivity for early detection of disease, because closer contact under higher pressure is more likely to induce friction sounds. It has been shown *ex vivo* based on cartilage samples taken from normal and pathological joints that knee AE is directly related to cartilage surface roughness [24].

Translating knee joint sounds into a clinical joint assessment tool requires validation against existing standards, such as those based on imaging techniques. Some investigators have reported association with categorical whole-joint grades of anatomic deterioration assessed by X-ray or MRI [25]-[28]. In this work we develop processing methodologies to permit direct association of specific AE features with specific types of anatomical damage. Although our focus is the relationship between knee AE and MRI, the proposed processing framework is extendable for assessing different types of knee joint sound and different imaging modalities.

3D measurements of knee articular cartilage using MRI provide biomarkers with proven accuracy, repeatability and reproducibility [29]. While AE provides a time-dependent but 1D signal reflecting the dynamic interaction among internal joint components, MRI provides many potential biomarkers from 3D images of static geometry and tissue composition (in terms of bone, cartilage, and meniscus in each compartment), so there are many potentially independent MRI-AE biomarker correlations that could be explored. Here we estimate local cartilage-on-cartilage areas according to knee joint angle for correlation with time- (and therefore angle-) dependent AE. Essentially, the approach extends previous work on MRI-based knee kinematics [30], whereby a dense 3D model of the knee is created from MRI and the femur bone is rotated with respect to the tibia bone to mimic knee joint movement. As femur rotation angle changes, different regions of femoral cartilage move onto the top of the tibial plateau, forming the angle-based tibiofemoral contact area, and enabling estimation of the articular cartilage thickness for each knee joint angle.

AE in the ultrasonic frequency range is less susceptible to motion artefact and environment noise than vibroarthrography and phonoarthrography [31]. The occurrence of AE events (also referred to as AE hits) and their transient waveforms correspond well to transient elastic stress waves generated by elastic cartilage deformation during weight-bearing translation of articular surfaces [24]. However, the AE hits and waveforms can be easily altered by a small movement variation, because a different weight redistribution can significantly affect elastic cartilage deformation. This is further complicated by multiple AE sources, because knees have multiple pairs of articulating surfaces. These issues present challenges to the aim of identifying knee AE features characteristic of particular MRI biomarkers. By assuming that AE acquired from a knee performing repeated movements should contain data which consistently reflect knee condition, a systematic processing framework is presented to derive statistically representative angle-based AE features from large numbers of AE hits. This involves identifying AE hits of interest by source-based waveform grouping, using angular sliding window to estimate the underlying variation of AE waveform features, and adjusting for unreliable AE acquisition based on weight-bearing asymmetry.

Having developed the methodologies to enable angle-based correlation between knee MRI and AE, we apply them to 10 OA knees to investigate the hypothesized association between AE and articular cartilage thickness, focusing on the MTF joint.

II. Methods

A. Participants

We studied 10 participants selected from our large population-based study to investigate AE biomarkers of OA knees [28]. Participants identified their worst knee as the index knee for this study. As shown in Table I (see Section III.A for assignment of knee ID), participants have ages from 55 to 79 years, body mass index (BMI) from 25.08 to 35.49 kg/m^2, and X-ray Kellgren-Lawrence (KL) scores [32] from 1 (indicating mild changes only) to 4 (indicating severe OA). Radiographs were acquired during standard care at a local NHS hospital, and KL scores were assessed and agreed independently by 2 experienced musculoskeletal radiologists. Although the number of participants was small due to the exploratory nature of the work with the main aim to establish the viability of the proposed processing methodologies, all possible KL scores were included to provide a range of cartilage damage for correlation with knee AE.

3D MRI and AE measurements of each OA knee were taken within one month of each other in local clinic environments. All subjects undertook only normal daily weight-bearing activities prior to AE measurements. Written consents were obtained prior to participation. The study was approved by the local NHS research ethics committee.

TABLE I
Individual Participant Demographics

Knee ID	Age	Gender	Height (m)	Weight (kg)	BMI (kg/m^2)	KL
K1	55	F	1.69	72	25.21	1
K2	63	F	1.66	79	28.67	3
K3	61	M	1.77	100	31.92	2
K4	79	F	1.61	65	25.08	2
K5	58	F	1.72	105	35.49	3
K6	73	F	1.65	71	26.08	2
K7	66	F	1.60	85	33.20	3
K8	66	M	1.66	78	28.31	4
K9	69	M	1.75	104.3	34.06	4
K10	69	M	1.68	71	25.16	3

B. Magnetic Resonance Imaging and Processing

MRI was performed at 3T as described previously [33]. Briefly, a water-selective sagittal 3D gradient recalled echo sequence was employed with repetition time (TR) of 15 ms, echo time (TE) of 5.6 ms, and nutation angle 25° produced images with 0.36×0.36 mm pixels and 0.7 mm slice thickness.

Processing of the volumetric knee images comprised two stages, with the first stage designed to construct accurate 3D surfaces of knee articular cartilage, and the second stage designed to estimate the angle-based cartilage thickness of the MTF contact area.

In the first stage, bone and cartilage of each knee were segmented by an experienced manual segmenter, using a semi-automated livewire algorithm (Endpoint segmentation software, Imorphics, Manchester, UK). This produced a set of contours, one for each slice of the MR image. 3D surfaces of femur, tibia, and patella, as well as four tibiofemoral cartilage regions (medial and lateral regions at the end of femur and at the top of tibia) were then generated from the stack of contours using a marching-cubes algorithm, followed by quadratic smoothing of the resultant surfaces.

In order for the same articular cartilage area to be selected from the mild and severe OA knees for meaningful pair-wise comparison, anatomical correspondence between their MRIs needs to be established based on a common reference frame. This was achieved by using active appearance models (AAMs) of the bones [34]. Previously, from an independent set of 96 knee MRIs acquired using the Siemens DESS-we sequence and containing approximately equal numbers for each KL score, 3D AAMs for femur, tibia and patella were built based on their mean shape and appearance as well as their principal modes of variation accompanied by a set of dense anatomical correspondences [35]. By using the previously constructed 3D AAMs to search automatically for similar structures in each knee, it produced another set of segmented bone surfaces for femur, tibia and patella fitted with a set of dense anatomical correspondence points (52,892 and 34,383 vertices for femur and tibia respectively, with points separated by around 1 mm).

From the above two processing steps, the bone surface of each knee exists in 2 representations, namely, the manual bone surface, and the AAM bone surface. The dense anatomical correspondence points from the AAM bone surface were transferred onto the manual bone surface by projecting normal from each correspondence point so as to intersect with the manual bone surface. This produced an accurate manual segmented bone surface fitted with a set of dense anatomical landmarks. At each anatomical landmark on each bone surface, cartilage thickness was measured as the distance to the manually-segmented outer cartilage surface along the bone surface normal, thereby forming a set of accurate 3D cartilage surfaces.

In the second stage to estimate the angle-based cartilage thickness of the MTF contact area, the medial and lateral epicondyles of the femur in each knee were located based on its bony protrusions to provide a pair of 3D reference coordinates, and they were then linked to form the epicondylar axis for rotation of femur with respect to tibia. In Fig. 1, the epicondylar axis is shown in red lying along the y-axis, with the x-axis in the inferior-superior direction, the z-axis in the anterior-posterior direction, and the origin of the 3D coordinate system at the lateral epicondyle point. Also illustrated in Fig. 1 is the approach implemented to locate the center of the medial tibial plateau, where the epicondylar axis is projected down to the tibial plateau (shown as parallel blue lines), and produces the elevation profile of the tibial plateau (shown as the trace along the ends of blue lines). With the medial tibial plateau known to be concave in shape, its width can be determined by searching its two edge points (shown by two blue dots) based on the shortest projection distances along the elevation profile in the medial half, thereby enabling the medial tibial plateau center (shown by the red dot) to be located as the midpoint of the medial tibial plateau width.

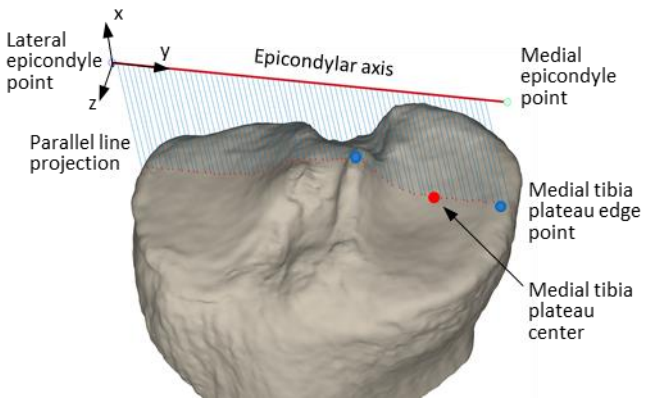

Fig. 1. Tibia elevation profile and medial compartment center

For computational simplicity, a circular patch around the medial tibial plateau center was defined as the MTF cartilage-on-cartilage contact area. Furthermore, this central contact area was assumed to be constant during knee joint movement, though it has been shown to change dynamically under loading [36]. Based on the findings from [37] with the medial cartilage contact area found to range from 104 to 176 mm^2 after 5 sec under full body weight, the radius of the circular patch was set to 30% of the medial tibial plateau width.

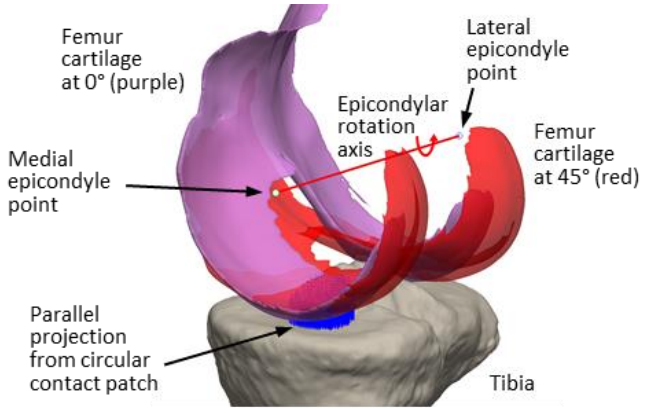

Fig. 2. Computation of angle-based medial femur cartilage thickness

While articular cartilage thickness on the central medial tibial plateau can be estimated by just one computation because it can be assumed to be independent of knee joint movement, multiple computations are required to estimate the medial femoral cartilage thickness because it is dependent on the knee joint angle, with different regions of the femur in contact with the tibia. For the former, estimation involved simple averaging of the distances between the surface points lying within the circular patch on the central medial tibial plateau and their corresponding points directly above on the central medial tibial cartilage surface. For the latter, estimation involved rotation of the femur according to the knee joint angle in the first instance.

After rotation of the femur cartilage around the epicondylar axis to correspond to a knee joint angle while maintaining the tibia stationary (with rotation from 0° to 45° illustrated in Fig. 2), the points lying within the circular patch on the central medial tibial plateau are projected upwards (shown as parallel blue lines from the tibial plateau to the femur cartilage in Fig. 2) to intersect with the outer and inner surfaces of the medial femur cartilage, enabling the medial femur cartilage thickness to be computed as the average distance among the corresponding pairs of the inner and outer cartilage surface points.

C. Knee Acoustic Emission and Processing

The hardware and software, sensor type and attachment, and movement protocol were based on previous work [23] which successfully differentiated healthy, aging and OA knees [38] [39]. The 'Joint Acoustic Analysis System' (JAAS) (Mistras Group) provided two AE channels for acquisition of knee AE as established in AE monitoring of engineering structures, two goniometer channels for acquisition of joint angles, and two footplates for acquisition of weight-bearing. The hardware was connected via USB to a laptop computer running the Mistras AEWin software for control and visualization of data acquisition.

The sensor types were S9024 piezoelectric AE sensors from Mistras and SG-150 strain gauge electro-goniometer (Biometrics Ltd). Each sensor was attached over the MTF compartment of each knee (inferior to the patella and anterior to the medial patella retinaculum) using 130×130 mm hypoallergenic medical adhesive tape. To ensure consistent contact with good ultrasonic coupling between the sensor surfaces and skin, a smooth and thin layer of Vaseline was applied to the ceramic face of the AE sensor before attachment. Each sensor was attached while each knee was supported in extension and the adhesive tape was applied to give the highest possible elastic tension to hold tightly each AE sensor over the MTF compartment. This prevents the AE sensor from sliding during joint movement, as joint flexion will create a greater elastic tension to press down further the AE sensor on the MTF compartment. A small hole was made in the middle of the tape to allow connection of the cable after sensor placement on the knee. The location and attachment of the electro-goniometers are not critical, and they were positioned laterally to each knee using double sided medical tape.

Repeated sit–stand–sit (SSS) movements were used as the movement protocol for measurement. With each foot on the center of each footplate, each participant was asked to ascend from a standard height chair, with arms folded across the chest (to minimize the influence of the arms in the movement strategy), pause for a second upon reaching a fully erect standing position, and then descend to return to a seated position. They were also asked to move at a usual and comfortable speed while looking ahead throughout. Each participant was asked to perform 2 SSS movements as warm-up before measurement, and a total of 10 SSS movements during measurement, through series of 5 consecutive movements with a 30 sec to 1 min break between each series.

While knee AE (20~400 kHz) was acquired at 5 MHz sampling frequency with the magnitude threshold to trigger recording of an AE hit set to 36 dB (around 63 μV), knee angle and weight-bearing signals were acquired at 20 Hz sampling frequency. Other relevant parameters for recording AE hit waveforms were Hit Definition Time (HDT) set to 800 μs for determination of the end of the hit (without merging two separate AE hits as one), Peak Definition Time (PDT) set to 200 μs for determination of the peak amplitude, and Hit Lockout Time (HLT) set to 1000 μs for inhibiting data acquisition after HDT.

Since people with unilateral knee OA may avoid pain by offloading on the affected side during SSS [40] and reduced joint loading may produce fewer AE hits with unrepresentative waveforms, a notional indicator of weight-bearing asymmetry (WBA) was calculated as a validity measure of AE data, with WBA computed as the ratio of "the average weight-bearing value from the OA knee in performing each series of SSS" divided by "the corresponding average weight-bearing value from the other knee". For WBA≤0.5 (corresponding to loading on the other knee to be at least twice higher on average), it was interpreted as insufficient weight loading on the OA knee with the acquired AE data unlikely to be representative of the internal knee condition.

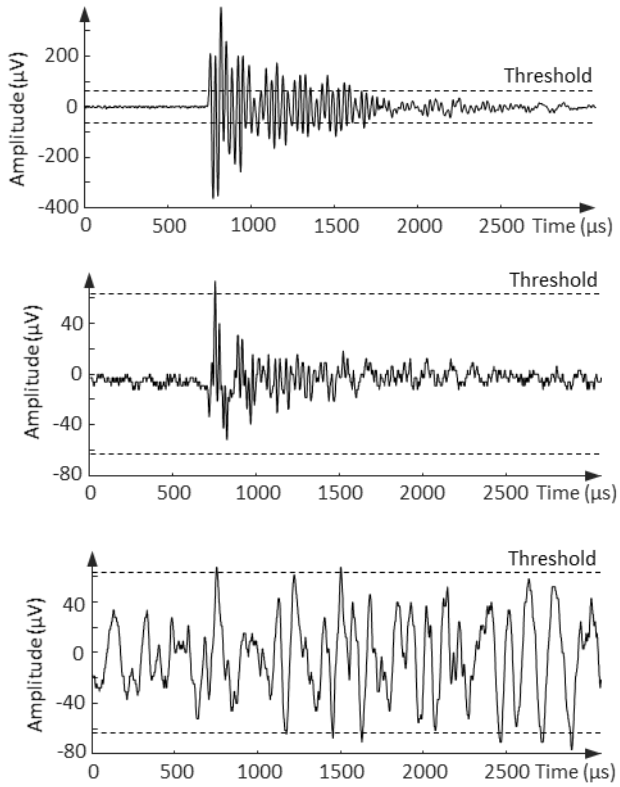

Fig. 3. Example AE waveforms: strong transient wave (top), weak transient wave (middle), and weak continuous wave (bottom)

In order to identify AE hits of interest, which should come from MTF articulation instead of other sources, particularly lateral tibiofemoral (LTF) and patellofemoral (PF) articulations, AE waveforms were analyzed based on waveform

shape and strength. From the perspective of motion, the waveform shape from the MTF and LTF articulations should be similar because they have the same motion of rolling, and different from the PF articulation because of its different motion of sliding. Furthermore, compared with the MTF articulation, the LTF and PF articulations should produce weaker AE signals because of lower loading [2] and higher attenuation due to a longer distance from the AE sensor. Hence, strong and weak transient waves were attributed to the MTF and LTF articulations respectively, with weak continuous waves attributed to the PF articulation. An example of each waveform type is illustrated in Fig. 3. The top example shows a strong transient wave with both positive and negative peaks significantly exceeding the AE detection threshold, the middle example shows a weak transient wave with only one peak slightly exceeding the AE detection threshold, and the bottom example shows a weak continuous wave with multiple peaks slightly exceeding the AE detection threshold.

Through source-based waveform grouping, AE hits generated by the MTF articulation were identified as those with peak amplitude values ≥40dB. This was followed by extraction of characteristic waveform features from each AE hit for correlation with the MTF cartilage thickness. Listed in Table II are the definitions of the waveform features extracted.

TABLE II
AE WAVEFORM FEATURES

Feature	Definition
Absolute energy (E_{abs})	$\int_{t_s}^{t_e} s(t)^2 dt/10k\Omega$ (aJ)
Average signal level (ASL)	$\sqrt{\frac{1}{T}\int_{t_s}^{t_s+T}(20log_{10}\left(\frac{s(t)}{1\mu V}\right)-G)dt}$ (dB)
Average frequency (f_a)	N_{AE}/T_{AE} (Hz)
Centroid frequency (f_c)	$\int fS(f)df/\int S(f)df$ (Hz)
Counts (N_{AE})	Number of threshold crossings from t_s to t_e
Counts-to-peak (N_P)	Number of threshold crossings from t_s to t_p
Counts-to-end (N_E)	N_{AE} - N_P
Duration (T_{AE})	t_e - t_s (μs)
Fall time (T_F)	T_{AE} - T_R (μs)
Initiation frequency (f_i)	N_P/T_R (Hz)
Peak amplitude (A_p)	Highest waveform amplitude (dB)
Peak frequency (f_p)	Frequency with maximum power (Hz)
Rise time (T_R)	t_p - t_s (μs)
Reverberation frequency (f_r)	N_E/T_F (Hz)
Root-mean-square (RMS)	$\sqrt{\frac{1}{T}\int_{t_s}^{t_s+T} s(t)^2 dt}$ (mV)
Signal strength (SS)	$\int_{t_s}^{t_e}\|s(t)\|dt$ (mV-μs)

aJ = attojoules, G = Gain of AE pre-amplifier in dB, $s(t)$ = AE signal, $S(f)$ = magnitude frequency spectrum of $s(t)$, T = Hit time frame, t_s = time of first threshold crossing, t_e = time of last threshold crossing, t_p = time of maximum amplitude.

If each SSS movement is treated as one individual test to give a particular outcome of AE measurement, one could expect a clear pattern reflecting the internal friction of tibiofemoral articulation to emerge from multiple AE measurements of repeated SSS movements. However, this does not happen since it is impossible for humans to perform identical SSS movements, particularly if they have knee OA. This has led to the use of an angular window sliding across each joint angle to capture the AE hits occurring around the similar angles in different SSS cycles, and the aggregated means of windowed AE hits and their features are taken as good measures of local cartilage articulation friction.

However, there is a dilemma in setting an appropriate angular window width, with a longer one likely to smooth out local changes and a shorter one likely to yield unreliable local estimate due to an insufficient number of hits. This was solved by setting the angular window width based on the average shift of the joint angle corresponding to the standing position.

Through angular sliding window to derive average number of AE hits and average value of each AE feature per cycle per angle from 10 SSS performed by each knee, angle-based correlation was followed to investigate their relationships with the corresponding MTF cartilage thickness of 10 OA knees computed from MRI, which involved non-parametric statistical tests based on the Spearman rank correlation coefficient (SRCC) with the significance level set to 5%.

III. RESULTS AND DISCUSSION

A. Joint Angle-based Cartilage Thickness

For the first stage of the 3D processing method presented in Section II.B, shown in Fig. 4 are examples of the final 3D knee models constructed for two knees with mild and severe OA respectively, where the cartilage surfaces are colored in red. From Fig. 4, the LTF compartments of both knees on the left are seen to have similar cartilage cover, whereas the MTF compartments of both knees on the right are seen to be significantly different with the femur region of the severe OA knee seen to have an area without cartilage cover leaving bone exposed.

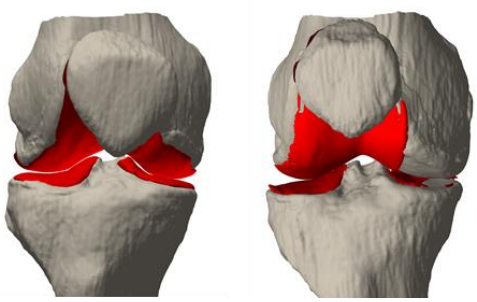

Fig. 4. 3D model of mild OA knee (left) and severe OA knee (right)

For the second stage of the 3D processing method presented in Section II.B, the cartilage-on-cartilage contact area of the MTF compartment of the 10 OA knees was found to be 123.95±31.40 mm^2 (mean ± standard deviation), and the average cartilage thickness of the central medial tibia plateau was 1.67±0.95 mm. Assuming the average tibia cartilage thickness to be invariant to joint angle, shown in Fig. 5 are the total MTF cartilage thickness profiles of the 10 OA knees by adding the average medial femur cartilage thickness at 1° resolution from 0° corresponding to standing to 90° corresponding to sitting, where K1~10 denote 10 OA knees according to the average medial tibia cartilage thickness from thickest to thinnest.

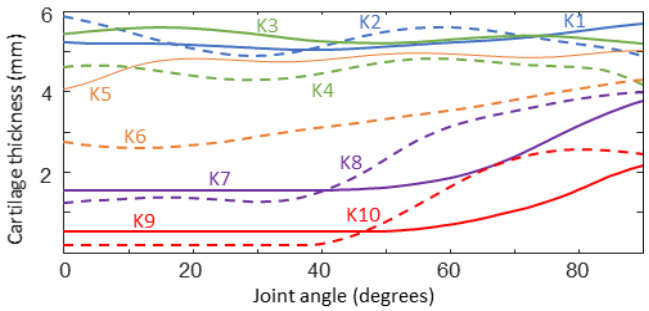

Fig. 5. Joint angle-based MTF cartilage thickness

Based on the cartilage thickness variation, two knee groups are evident, with K1~5 having relatively high and constant cartilage thickness throughout the whole angular range (>4 mm), and K6~10 having cartilage thickness which decreases from a relatively thick level around the sitting position at 90° to a thin level as joint angle decreases (<2 mm for K7~10). With the MTF joint constantly required to support high loads around the standing position during daily activities, such cartilage loss is a recognized feature of knee OA [42].

B. Acoustic Emission Events

Shown in Fig. 6 are examples of the data acquired from mild and severe OA knees performing 5 SSS. Plotted against the left-axis is joint angle-based AE with AE hits (shown as black dots) superimposed on joint angle signal (shown as blue curves), and plotted against the right-axis is the variation of weight-bearing as percentage of body weight (BW) (shown as red curves). From Fig. 6, it is apparent that the number of AE hits from the severe OA knee is significantly higher than from the mild OA knee, indicating more friction between the internal articulating surfaces.

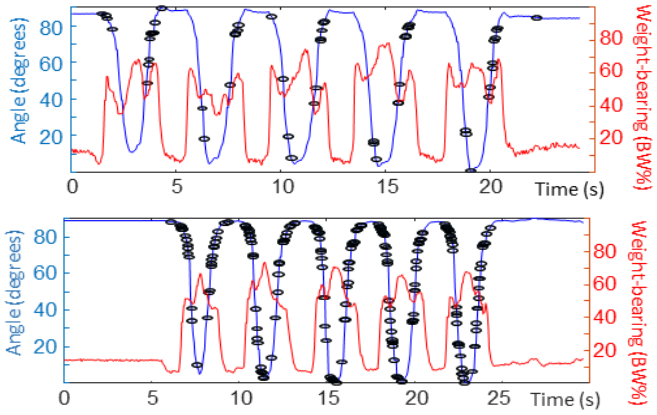

Fig. 6. Knee AE from mild OA (top) and severe OA (bottom)

In Fig. 6, the highest and lowest joint angles in each SSS cycle correspond to the knee flexion angle at the sitting position and knee extension angle at the standing position respectively, whilst the decrease and increase in the joint angle in each SSS cycle correspond to the ascending (sit-to-stand) phase and the descending (stand-to-sit) phase respectively. Due to inherent movement variation between cycles [41], both joint angle and weight-bearing signals are seen to vary slightly from cycle to cycle. Nevertheless, the variation of weight-bearing generally moves in the opposite direction to joint angle, with lowest weight-bearing at the sitting position and highest weight-bearing at the standing position.

To assist fair comparison of AE from different OA knees, WBA was checked to ensure similar weight-bearing conditions during SSS, and a marked difference was found between K10 with WBA<0.5 and other knees with WBA of 1.21±0.14, implying significant offloading on the affected knee by this participant. As shown in Fig. 5, K10 had the thinnest MTF cartilage, which is almost zero for joint angles from 0° to 40°, supporting the possibility that this participant may adopt a movement strategy to markedly reduce weight bearing of the affected knee during SSS. Therefore, the AE data of K10 is unlikely to be consistent with its group.

In addition to weight-bearing, SSS speed is another factor with a potential cofounding effect on knee AE. Within subjects, the variation in SSS cycle time was within the range of 0.5~2 sec for all knees, except K10 reaching almost 3 sec and indicating low repeatability of SSS cycles. Between subjects, the time taken to complete each SSS cycle was within the range of 2~5.5 sec for all knees, except K10 requiring significantly longer time of 6.5~9 sec and providing further support to asymmetric loading during SSS. Since the SSS variability within and between subjects of all knees except K10 was on a par with the range of the previous work [39], it can be assumed to be sufficiently low with negligible effect on AE measurement outcomes.

As a result of significant differences with respect to other knees on weight-bearing and movement speed, K10 appears as an outlier in terms of the average number of AE hits/cycle, which is 14.6 hits/cycle, around two standard deviations below the average of its group members of K6~9 with 32.2±9.5 hits/cycle. With thicker cartilage, the average number of AE hits/cycle of K1~5 is less than the average of K6~9 by approximately 36%, with 20.6±11.0 hits/cycle, reflecting less internal articulation friction.

By splitting each SSS cycle into the ascending and descending phases, the average number of AE hits/phase of K1~5 is again less than K6~9 for both phases, with 10.1±6.7 hits/phase against 15.9±6.0 hits/phase in the ascending phase, and with 10.5±5.0 hits/phase against 16.3±4.9 hits/phase in the descending phase. Also, K10 had 2.9 hits/phase for ascending and 11.7 hits/phase for descending on average, suggesting an offloading strategy in standing up.

C. Association of Acoustic Emission Events and Cartilage

With 4.3° found to be the average shift of the joint angle at the standing position among the participants, a sliding angular window with a width of ±5° centered at every degree was implemented. Fig. 7 shows the AE hit distribution of the 10 OA knees for the complete SSS movement as a heatmap, with colors from dark blue to bright yellow denoting the increasing hit density in terms of the average number of AE hits per cycle per angle. Comparing the left half for the ascending phase (from 90° to 0°) with the corresponding right half for the descending phase (from 0° to 90°), the AE hit distribution of each knee is not symmetrical with different variation patterns, implying different friction behaviors between ascending and descending

as one would expect. Comparing the top half of K1~5 with the bottom half of K6~10, the latter tends to be brighter (except the ascending phase of K10 where offloading has been identified) indicating a higher hit density as a result of more articulation friction due to thinner cartilage thickness.

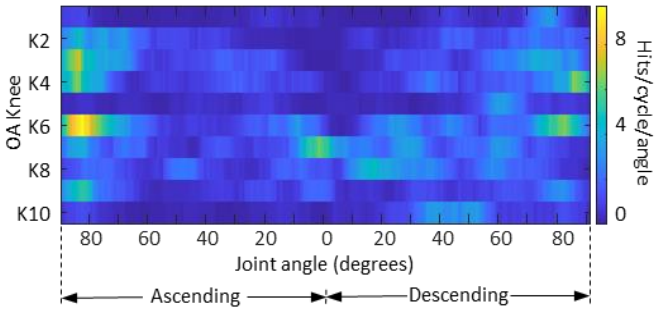

Fig. 7. Joint angle-based hit density of 10 OA knees (with color variation along each row showing averaged number of hits against joint angle of each knee during SSS)

With both MTF cartilage thickness and AE hit density related to joint angle as shown in Figs. 5 and 7, direct correlation of them was performed at each joint angle in each movement phase with K10 excluded as an outlier. Highest negative correlation was found to occur around the standing position with SRCC value of -0.92 and *p*-value of 0.0012, indicating a strong inverse association between the ranked values of cartilage thickness and hit density. This finding is significant, because it points to the knee angle of 0° that is most exposed to wear with the widest spread of cartilage thickness among the participants. It is also consistent with the physical phenomenon of higher MTF friction from knees with thin cartilages when moving around the standing position under full body weight.

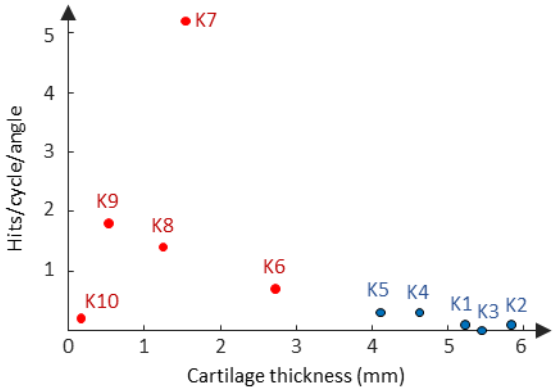

Fig. 8. MTF cartilage thickness versus hit density at 1° of descending

Shown in Fig. 8 is the scatter plot of MTF cartilage thickness and windowed hit density at 1° joint angle at the start of the descending phase, with K1~5 denoted by blue dots and K6~10 denoted by red dots. K10 is seen to go against the physical behavior pattern expected, because its hit density should be higher than K1~5, and close to K6~9 with more friction-induced AE as a result of having the thinnest articular cartilage, this could only be explained by significant offloading to reduce articulation friction as evidenced by its low WBA ratio. More significantly, there appears to be a trend of less friction-induced AE hits as cartilage thickness increases (from K9 at around 0.5 mm to K2 at almost 6 mm) based on 8 out of 10 knees.

D. Association of Acoustic Emission Features and Cartilage

The same approach was used to correlate each AE feature (with definitions provided in Table II) with MTF cartilage thickness to investigate possible relationships. With K10 excluded as an outlier, the entire set of the correlation results based on SRCC is presented in Fig. 9 as a heatmap, where bright yellow and dark blue indicate respectively positive and negative correlations with greenish color indicating no association between the ranked values of cartilage thickness and the windowed AE feature means. For each AE feature, the joint angle with highest magnitude values of SRCC and corresponding *p*-value are listed in Table III.

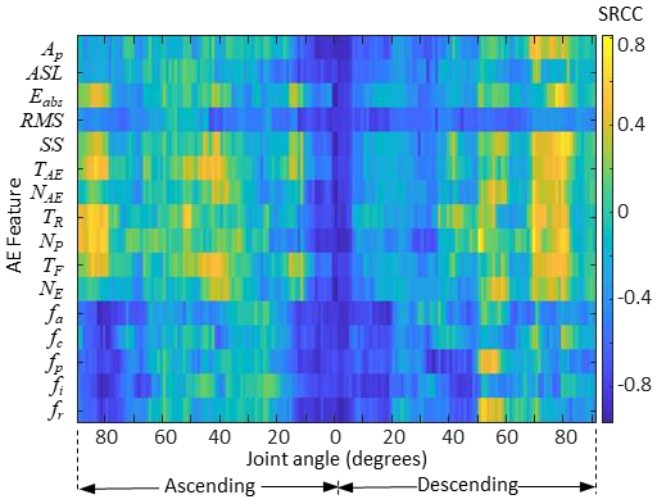

Fig. 9. Joint angle-based SRCC heatmap

TABLE III
HIGHEST CORRELATIONS BETWEEN AE AND CARTILAGE THICKNESS

AE Feature	Joint Angle	SRCC	*p*-value
A_p	0°	-0.9167	0.0013
ASL	1° (descending)	-0.9000	0.0020
E_{abs}	0°	-0.9667	1.6534×10^{-4}
RMS	2° (ascending)	-0.8500	0.0061
SS	0°	-0.9667	1.6534×10^{-4}
T_{AE}	1° (ascending)	-0.8500	0.0061
N_{AE}	0°	-0.9667	1.6534×10^{-4}
T_R	0°	-0.9167	0.0013
N_P	1° (descending)	-0.9205	0.0010
T_F	1° (ascending)	-0.8500	0.0061
N_E	0°	-0.9667	1.6534×10^{-4}
f_a	83° (ascending)	-0.9333	7.4956×10^{-4}
f_c	80° (ascending)	-0.9167	0.0013
f_p	34° (descending)	-0.9167	0.0013
f_i	82° (ascending)	-0.9333	7.4956×10^{-4}
f_r	1° (descending)	-0.9333	7.4956×10^{-4}

As shown in Fig. 9, none of the AE features have a color variation pattern with left-right symmetry, indicating again two different friction behaviors between ascending and descending motions. Although there are yellow and blue patches appearing at different joint angles for different AE features indicating the existence of various positive and negative correlations, the

magnitude of the most negative correlation is noted to be higher than that of the most positive correlation, with almost -1 against a value around 0.8, indicating inverse associations to be stronger. This is also supported by Table III where the highest SRCC for all AE features are seen to be negative. Most significantly, the biggest blue patch is seen to occur at joint angle around 0° across all AE features in the middle of Fig. 9, and 12 out of 16 AE features are seen to have highest SRCC around 0° in Table III. This reaffirms the previous findings based on hit density by also suggesting the fully standing position as the most informative joint angle for association of AE measurement with cartilage thickness, and provides additional AE waveform features to support the previous physical interpretation of higher hit density as a result of greater articulation friction from knees with thinner cartilages under full body weight, which include higher amplitude, longer duration, greater energy and increased frequencies.

Depending on AE feature type, negative correlation with MTF cartilage thickness around 0° joint angle varies from a moderate level of around -0.7 to a strong level of almost -1, shown in Fig. 10 are two scatter plots of 5 AE features with highest SRCC and lowest *p*-values around 0° in Table III to illustrate the goodness of correlation.

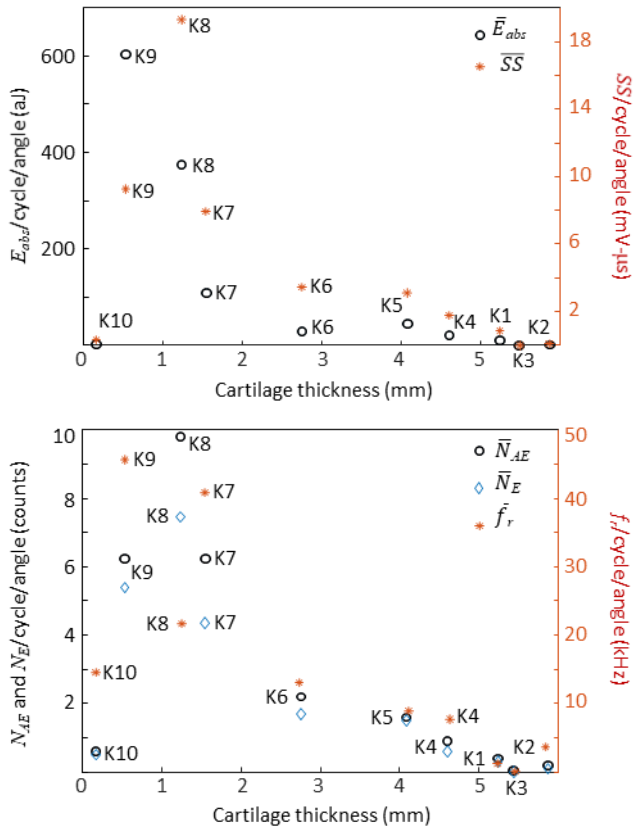

Fig. 10. Cartilage thickness versus E_{abs} and *SS* at 0° (top), versus N_{AE} and N_E at 0°, and f_r at 1° of descending (bottom)

In Fig. 10 (top) with cartilage thickness as the x-axis, the windowed absolute energy per cycle per angle ($\overline{E}_{abs}$) of each knee is denoted by black 'o' and plotted against the left-axis, whereas the windowed signal strength per cycle per angle ($\overline{SS}$) of each knee is denoted by red '∗' and plotted against the right axis. With both features indicating the level of internal friction, K10 is clearly seen to be an outlier, and it shows that offloading around WBA≈0.5 can reduce the friction energy and strength inside a knee with thinnest cartilage to a level compatible to a knee with the thickest cartilage. If K10 is ignored as an outlier, then there appears to be a pattern of exponential decay to indicate less friction energy and strength as the MTF cartilage thickness increases, with just one exception for $\overline{E}_{abs}$ at the boundary of the two groups where K6 is seen to have lower $\overline{E}_{abs}$ than K5, and with a different exception for $\overline{SS}$ at the thinnest cartilage end where K9 is seen to have lower $\overline{SS}$ than K8. Since both $\overline{E}_{abs}$ and $\overline{SS}$ are proportional to amplitude and duration as shown in Table II, it implies friction-induced AE hits from knee with thin cartilage tend to have higher peak amplitude and longer duration. Also from Table III, E_{abs} and *SS* are higher than A_p and T_{AE} in magnitude, indicating a potential of achieving higher correlation via composite feature descriptors.

In Fig. 10 (bottom), the windowed threshold-crossing counts and counts-to-end per cycle per angle ($\overline{N}_{AE}$ and $\overline{N}_E$) of each knee are denoted by black 'o' and blue '◊' respectively, and plotted against the left-axis. Again regarding K10 as an outlier, both $\overline{N}_{AE}$ and $\overline{N}_E$ have the same exponential decay pattern as $\overline{SS}$, indicating the tendency of knees with thinner cartilages to generate AE hits with more intensive transient oscillation throughout the waveform duration, especially in the downward falling section.

Also in Fig. 10 (bottom), the windowed reverberation frequency per cycle per angle ($\overline{f}_r$) of each knee is denoted by red '∗', and plotted against the right axis. K10 is less of an outlier for this AE feature, suggesting the effect of offloading to be more significant on friction magnitude and less significant on friction frequency. If K10 is again regarded as an outlier, the overall decay pattern of $\overline{f}_r$ is similar to exponential, indicating the tendency of knees with thinner cartilages to generate AE hits with higher reverberation frequencies as a result of increased articulation friction. As shown in Table III, although the SRCC value of f_r has smaller magnitude than the other four AE features in Fig. 10, it is the most significant feature at 0° joint angle among all frequency related features.

E. Discussion and Limitations

From the exploratory results based on 10 OA knees, the viability of the proposed processing framework as a new approach for discovery and validation of AE biomarkers has been demonstrated.

In developing the methodology for processing knee MRI to estimate joint angle-based cartilage thickness, several simplifications have been made to enable computation. These include use of the simplest knee kinematics to model the SSS movement with just one directional rotation and an assumption of a fixed contact area between femur and tibia articular cartilages. Although the joint angle-based cartilage thickness profiles shown in Fig. 5 could vary if the location and size of the cartilage contact area are changed as a result of using more complex kinematics and different radius, the changes are

unlikely to cause significant variations, since the influence on cartilage thickness calculated as an average over two contact surfaces at each joint angle is more likely to be small, and it is even more unlikely to change the ranked order of the cartilage thickness at 0° as well as the corresponding correlation results at the fully standing position.

Translation of AE from industrial non-destructive monitoring of engineering structures to medical non-invasive monitoring of knee joints needs to address the variability of the *in vivo* measurement, since movement and weight-bearing are required to trigger AE [18]. Based on the measurement results of 10 OA knees containing both large and small variabilities, the proposed methodology has shown to be effective. While large variabilities were mitigated by using weight-bearing asymmetry and movement speed to identify K10 as an outlier, small variabilities were seen to be overcome by the use of an angular sliding window (with the window width set to the expected movement-induced angular variation in multiple SSS) to reveal the underlying statistical trends of AE hits and features from K1~9.

In terms of the potential in applying the proposed processing framework for discovery of biomarkers, physically meaningful results have emerged, illustrating the advantages of using joint angle for associating knee AE and imaged anatomical features. In particular, from the results of joint angle-based correlation between the MTF cartilage thickness and AE hits as well as AE features of K1~9 through the full angular range of SSS, highest correlations were found to occur around the fully standing position at 0°. This is physically significant, because it corresponds to the condition of maximum difference in articulation friction among the participants, as a result of maximum anatomical difference in cartilage thickness (as shown at 0° of Fig. 5) and maximum weight-bearing (as shown at each fully standing position of SSS movements in Fig. 6). Under this condition, the spreads of AE hits and feature values are maximized, making 0° as an informative angle with high sensitivity to small differences in knee articulation friction. Further significance of the correlation results at 0° for all AE features is direction and strength, with SRCC values found to vary from -0.7 to almost -1. This suggests that thinner articular cartilages cause greater knee articulation friction, which in turn causes more AE hits with higher amplitude, longer duration, greater energy, and higher frequencies.

A striking discovery from our exploratory work is the shape of all inverse relationships shown in Figs. 8 and 10, where similar decreasing patterns of AE hits and features as cartilage thickness increases for joint angle around 0° are seen to have a shape that is consistent with the exponential law of friction [43].

Due to the exploratory nature of the work, preliminary validation of the proposed processing framework was based on a small number of participants with the limitation of small sample size. Although this problem has been mitigated by selecting participants with a full range of KL, it is likely that some participants may have unrecognized anatomical damage elsewhere in the knee joint, causing deviation from the trend, perhaps illustrated by the greater number of AE hits from K7 shown in Fig. 8.

One relevant anatomical compartment is the meniscus which was ignored in this work. As another weight-bearing structure, meniscal damage is likely to increase articulation friction at the cartilage-meniscus interface during SSS, causing significant AE.

With the focus on demonstrating the viability of the proposed processing framework, analysis of the relationships between knee AE and cartilage thickness has been limited to the fully standing position. There remain many relationships to be discovered across all other joint angles in both ascending and descending phases, and more sophisticated analysis methods could be adapted for further investigation, such as using the approach based on Principal Component Analysis as reported in the previous work on knee AE [39].

IV. Conclusion

This paper reports the first study to explore associations between anatomical biomarkers in knee MRI and waveform biomarkers in knee AE. We have focused on proposing a methodological framework for processing static 3D MRI and dynamic 1D AE to enable correlations between them to be explored based on joint movement angle, and demonstrating the viability of the proposed framework through an initial study of 10 OA knees.

Through joint angle-based correlation between the MTF cartilage thickness from MRI and knee AE from SSS movements, the potential of the proposed processing framework for biomarker discovery and validation is well illustrated, as evidenced by physically plausible results. In particular, joint angle at the fully standing position was found to be the most informative angle for AE-based measurement of cartilage condition, where thinner articular cartilages were found to generate more AE with higher amplitude, greater energy, longer duration, and higher frequencies, corresponding well to the underlying physical phenomenon of more intense articulation friction under full body weight.

Of most clinical significance is the possibility to use the proposed processing framework to establish accurate and robust relationships between AE features and cartilage thickness at all joint angles from the statistical trends over large numbers of knees. This could provide cost-effective non-invasive AE biomarkers of knee joint damage for patient stratification, prognosis, monitoring and response assessment in clinical trials.

Acknowledgment

We acknowledge the valuable input into this study from MISTRAS on JAAS equipment, local NHS organizations, and the participants. Dr M Dixon and J Huddleston provided project management support. Dr L Spain collected the AE data.

References

[1] H.K. Gahunia et al., (eds) *Articular Cartilage of the Knee,* Springer, 2020.
[2] D.D. D'Lima et al., "Knee joint forces: Prediction, measurement, and significance", *Proc. Inst. Mech. Eng. H,* vol. 226, no. 2, pp. 95–102, 2012.
[3] T.P. Andriacchi et al., "A framework for the in vivo pathomechanics of osteoarthritis at the knee," *Ann. Biomed. Eng.*, vol. 32, no. 3, pp. 447-457, 2004.
[4] R.K. Jones et al., "A new approach to prevention of knee osteoarthritis: Reducing medial load in the contralateral knee," *J. Rheumatol*., vol. 40, no. 3, pp. 309-315, 2013.
[5] L. Spain et al., "Biomarkers for knee osteoarthritis: New technologies, new paradigms," *Int. J. Clin. Rheumatol.*, vol. 10, no. 4, pp. 287-297, 2015.

[6] National Institute for Heath and Care Excellence (2014). Osteoarthritis: care and management in adults. [Online]. Available: www.nice.org.uk/guidance/cg177/resources/guidanceosteoarthritis-pdf

[7] D.J. Hunter et al., "Structural correlates of pain in joints with osteoarthritis," *OA & Cartilage*, vol. 21, no. 9, pp. 1170–1178, 2013.

[8] F. Eckstein et al., "Magnetic resonance imaging (MRI) of articular cartilage in knee osteoarthritis (OA): Morphological assessment," *OA & Cartilage*, vol. 14, Suppl. A, pp. A46–A75, 2006.

[9] C. Peterfy et al., "Workshop for consensus on osteoarthritis imaging: MRI of the knee," *OA & Cartilage*, vol.14, pp. 44–45, 2006.

[10] M.F. Sowers et al., "Magnetic resonance detected subchondral bone marrow and cartilage defect characteristics associated with pain and X-ray-defined knee osteoarthritis," *OA & Cartilage*, vol. 11, no. 6, pp. 387–393, 2003.

[11] T.M. Link et al., "Osteoarthritis: MR imaging findings in different stages of disease and correlation with clinical findings," *Radiology*, vol. 226, no. 2, pp. 373–381, 2003.

[12] A.E. Wluka et al., "The clinical correlates of articular cartilage defects in symptomatic knee osteoarthritis: A prospective study," *Rheumatology*, vol. 44, no. 10, pp. 1311–1316, 2005.

[13] L.M. Wildi et al., "Relationship between bone marrow lesions, cartilage loss and pain in knee osteoarthritis: Results from a randomised controlled clinical trial using MRI," *Ann. Rheum. Dis.*, vol. 69, no. 12, pp. 2118–2124, 2010.

[14] S. J. Song et al., "Noise around the knee", *Clin. Orthop. Surg*., vol. 10, no. 1, pp. 1-8, 2018.

[15] R. E. Andersen et al., "A review of engineering aspects of vibroarthography of the knee joint," *Crit. Rev. Phys. Rehabil. Med*., vol. 28, nos. 1–2, pp. 13–32, 2016.

[16] H. M. Bassiouni, "Phonoarthrography: A new technique for recording joint sounds," in *Osteoarthritis: Diagnosis, Treatment and Surgery*, InTech, 2012, ch. 16, pp. 275-288.

[17] K.A. Olorunlambe et al., "A review of acoustic emission as a biotribological diagnostic tool", *Tribology - Materials, Surfaces & Interfaces*, vol. 13, no. 3, pp. 161–171, 2019.

[18] L. Khokhlova et al., "Assessment of hip and knee joints and using acoustic emission monitoring: a scoping review", *IEEE Sensors J*., vol. 21, no. 13, pp. 14379-14388, 2021.

[19] G.-H. Feng and W.-M. Chen, "Piezoelectric-film-based acoustic emission sensor array with thermoactuator for monitoring knee joint conditions", *Sens. Actuators A: Phys*., vol. 246, pp. 180-191, 2016.

[20] C. N. Teague et al., "Novel methods for sensing acoustical emissions from the knee for wearable joint health assessment", *IEEE Trans. Biomed. Eng*., vol. 63, no. 8, pp. 1581-1590, 2016.

[21] K. Kaloa et al., "The detection of knee joint sounds at defined loads by means of vibroarthrography", *Clin. Biomech*., vol. 74, pp. 1-7, 2020.

[22] S. Gharehbaghi et al., "Acoustic emissions from loaded and unloaded knees to assess joint health in patients with juvenile idiopathic arthritis", *IEEE J. Biomed. Health Inform.*, vol. 25, no. 9, pp. 3618-3626, 2021.

[23] B. Mascaro et al., "Exploratory study of a non-invasive method based on acoustic emission for assessing the dynamic integrity of knee joints," *Med. Eng. & Phys.*, vol. 31, no. 8, pp. 1103-1022, 2009.

[24] K. Wierzcholski, "Acoustic emission diagnosis for human joint cartilage diseases," *Acta Bioeng. Biomech*., vol. 17, no. 4, pp. 139–148, 2015.

[25] M. T. Nevalainen et al., "Acoustic emissions and kinematic instability of the osteoarthritic knee joint: comparison with radiographic findings," *Sci. Rep*., vol.11, article 19558, 2021.

[26] T.I. Khan et al., "Research on diagnosis of knee osteoarthritis using acoustic emission technique", *Acoust. Sci. & Tech*. vol.42, no.5, pp. 241-251, 2021.

[27] J. Kiselev et al., "Detection of osteoarthritis using acoustic emission analysis", *Med. Eng. & Phys*., vol. 65, pp. 57–60, 2019.

[28] D.K. Schluter et al., "Use of acoustic emission to identify novel candidate biomarkers for knee osteoarthritis (OA)". *PLoS ONE*, vol.14, no.10, e0223711, https://doi.org/10.1371/journal. pone.0223711, 2019.

[29] M.A. Bowes et al., "Precision, reliability and responsiveness of a novel automated quantification tool for cartilage thickness: Data from the osteoarthritis initiative", *J. Rheumatol*. vol. 47, no. 2, pp. 282-289, 2020.

[30] L.-K. Shark et al., "Acoustic emission sonification and magnetic resonance imaging-based kinematics for exploratory analysis of Knee Joints," in *Proc. IEEE BIBM, Shenzhen, China*, 2016, pp. 1016-1022.

[31] A.O. Posatskiy and T. Chau, "The effects of motion artifact on mechanomyography: a comparative study of microphones and accelerometers," *J. Electromyogr. Kinesiol*., vol. 22, pp. 320-324, 2012.

[32] J.H. Kellgren and J.S. Lawrence, "Radiological assessment of osteo-arthrosis," *Ann. Rheum. Dis*. Vol. 16, no. 4, pp. 494–502, 1957.

[33] S. Balamoody et al., "Comparison of 3T MR scanners in regional cartilage-thickness analysis in osteoarthritis: A cross-sectional multicenter, multivendor study", *Arthritis Res. Ther*. vol. 12, no. 5, R202, https://doi.org/10.1186/ar3174, 2010.

[34] T.G. Williams et al., "Anatomically corresponded regional analysis of cartilage in asymptomatic and osteoarthritic knees by statistical shape modelling of the bone," *IEEE Trans. Med. Imaging*, vol. 29, no. 8, pp. 1541-1559, 2010.

[35] M.A. Bowes et al., "A novel method for bone area measurement provides new insights into osteoarthritis and its progression," *Ann. Rheum. Dis*., vol. 74, no. 3, pp. 519-525, 2015.

[36] C.S. Shin et al., "In vivo tibiofemoral cartilage-to-cartilage contact area of females with medial osteoarthritis under acute loading using MRI," *J. MRI*, vol. 34, pp.1405–1413, 2011.

[37] A. Hosseini et al., "In-vivo time-dependent articular cartilage contact behavior of the tibiofemoral joint," *OA & Cartilage*, vol. 18, pp. 909-916, 2010.

[38] L.-K. Shark et al., "Discovering differences in acoustic emission between healthy and osteoarthritic knees using a four-phase model of sit-stand-sit movements", *Open Medical Informatics Journal*, vol. 4, pp. 116-125, 2010.

[39] L.-K. Shark et al., "Knee acoustic emission: A potential biomarker for quantitative assessment of joint ageing and degeneration," *Med. Eng. & Phys*., vol. 33, no. 5, pp. 534–545, 2011.

[40] C.L. Christiansen and J.E. Stevens-Lapsley, "Weight-bearing asymmetry in relation to measures of impairment and functional mobility for people with knee osteoarthritis," *Arch Phys Med Rehabil* vol 91, pp. 1524-1528, 2010.

[41] L.-K. Shark et al., "Acoustic emission and angular movement variations from early adulthood healthy knees to late adulthood osteoarthritic knees," in *Proc. EMBC, Orlando, USA*, 2016, pp. 2382-2385.

[42] J.M. Johnson and M.R. Mahfouz, "Cartilage loss patterns within femorotibial contact regions during deep knee bend," *J. Biomech*., vol. 49 pp. 1794–1801, 2016.

[43] J. Awrejcewicz and P. Olejnik, "Analysis of dynamic systems with various friction laws," *Appl. Mech. Rev*., vol. 58, no. 6, pp. 389–411, 2005.